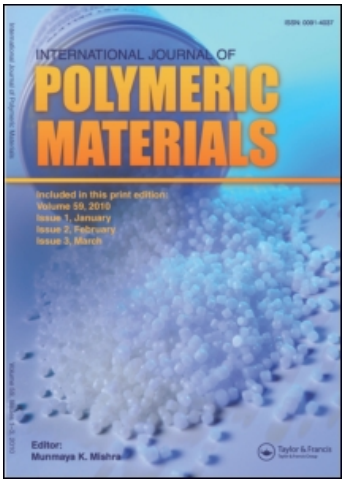

International Journal of Polymeric Materials
Publication details, including instructions for authors and subscription information:
http://www.informaworld.com/smpp/title~content=t713647664

Molecular Orientational States and Optical Properties of Surface-Stabilized Ferroelectric LCs

Nobuyuki Itoh[a]
[a] Functional Devices Laboratories, SHARP Corp., Chiba, Japan

To cite this Article Itoh, Nobuyuki(2000) 'Molecular Orientational States and Optical Properties of Surface-Stabilized Ferroelectric LCs', International Journal of Polymeric Materials, 45: 3, 349 — 380
To link to this Article: DOI: 10.1080/00914030008035049
URL: http://dx.doi.org/10.1080/00914030008035049

Intern. J. Polymeric Mater., 2000, Vol. 45, pp. 349–380
Reprints available directly from the publisher
Photocopying permitted by license only

Molecular Orientational States and Optical Properties of Surface-Stabilized Ferroelectric LCs

NOBUYUKI ITOH *

Functional Devices Laboratories, SHARP Corp. 273-1 Kashiva, Kashiva, Chiba 277, Japan

(Received 18 December 1998)

Ferroelectric liquid crystals are analyzed from the point of view of their surface stabilization. Device structure, memory effect and the viewing angle are defined. Smectic layers structures are investigated, including the relationship between the molecular tilt angle and the chevron layer tilt angle. Experimental results are reported for molecular orientational states in relation to optical properties.

Keywords: Ferroelectric liquid crystals; ferroelectric surface stabilization; device structure; memory effect; smectic layer structures; molecular tilt angle; chevron layer tilt angle; molecular orientational states; optical properties of liquid crystals

1. INTRODUCTION

A study of the molecular orientational states and the optical properties of surface stabilized ferroelectric liquid crystals (SSFLCs) is introduced in this section. The molecular orientational models were presented and they gave us a total understanding of the orientational states which appear in SSFLCs with the parallel rubbing and their optical properties. The smectic layer structure of various SSFLCs were studied by using the high resolution X-ray. The relationship between the layer tilt angle of the chevron structure and the optical molecular tilt angle was confirmed. The molecular orientational states of SSFLCs

*e-mail: itoh@ks1.kasiwa.sharp.co.jp

were classified by the optical viewing conditions and the relationship between the directions of the chevron layer structure and the surface pretilt. The molecular orientational models of the states were considered and illustrated with regard to the experimental results. The useful information from the optical simulations using the models was obtained. The effect of the surface pretilt angle on the orientational and the optical properties of SSFLCs was discussed.

The conception and the procedure of the study which includes the X-ray diffraction, the spectroscopic analysis, the optical simulation based on the molecular orientational models and the director profile, will also be useful for study of polymer liquid crystals because the molecular orientation of any types of liquid crystal device, of course polymer liquid crystals must be responsible for their optical properties. Therefore author believe that this section must be interesting for the research of polymer liquid crystals.

First, ferroelectric liquid crystals (FLCs) and SSFLCs which are the most interesting application of FLCs and their characteristics are briefly explained.

2. FERROELECTRIC SmC* LIQUID CRYSTALS

The chiral smectic C (SmC*) phase is well known as a representative liquid crystal phase showing ferroelectricity. Smectic A (SmA) and smectic C (SmC) are the fundamental phases among the smectic liquid crystal phases. As shown in Figure 1, the director **n** is parallel to the smectic layer normal Z in SmA phase and it is a uniaxial phase optically and dielectrically, on the other hand the director **n** tilts at the tilt angle θ from the smectic layer normal in SmC phase and it is a biaxial phase. In SmC* phase which is SmC phase having the chiral molecules but racemi, the helical structure with a constant tilt angle θ but slight different azimuthal angle Φ in each layer appears as shown in Figure 2 because of the chirality of molecules. Although a pitch is expressed by only four layers in Figure 2, an actual pitch is formed by more than several hundred layers. FLC molecules are placed on the smectic cone and moved around it.

The spontaneous polarization is originated in C_2 symmetry of SmC* phase perpendicular to the long molecular axis. The molecular

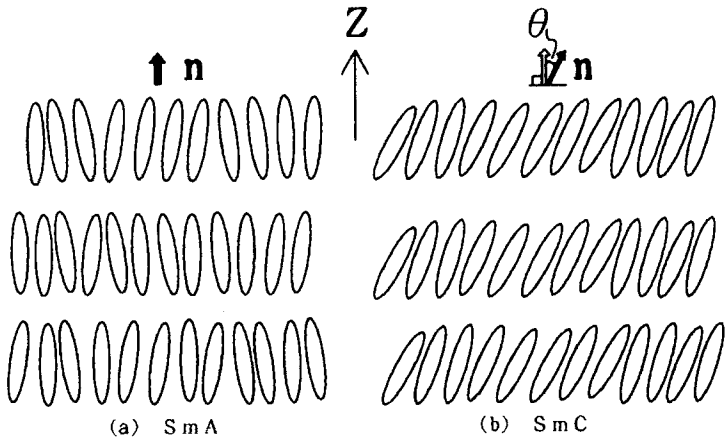

FIGURE 1 The molecular orientation of smectic phases.

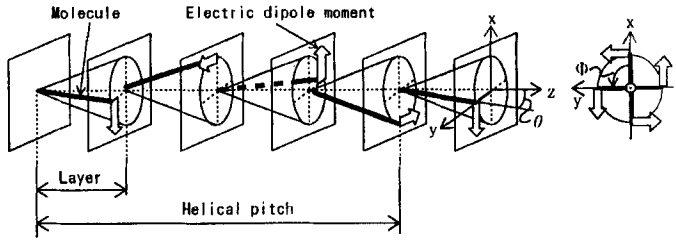

FIGURE 2 The molecular orientation of SmC* phase.

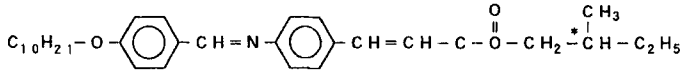

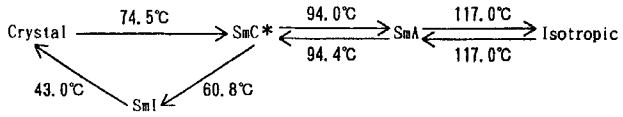

FIGURE 3 The molecular structure and phase sequence of DOBAMBC.

structure and the phase sequence of world first FLC, DOBAMBC (*p*-decyloxybenzylidene-*p'*-amino-2-methylbutyl-cinnamate) which was synthesized by Meyer *et al.* [1] is shown in Figure 3.

3. SURFACE STABILIZED FERROELECTRIC LIQUID CRYSTALS (SSFLCs)

3.1. Device Structure

The free rotation around the long molecule axis is hindered by chiral parts such as *C in Figure 3. The origin of the spontaneous polarization is this hindered rotation. The helical structure is formed by the chirality of the molecules and the frexoelectricity, but it is not necessary for the spontaneous polarization. Therefore the spontaneous polarization remains if the structure is unwound. Clark and Lagerwall [2] reported that the helix unwinding structure was realized by surface pinning effect using thin cell spacing less than 2 μm. It is called the surface stabilized state. The cell spacing is quite thin in comparison with the conventional nematic devices. Figure 4 shows the helix unwinding structure. There are two domains which are tilted at $\pm\theta$ from the smectic layer normal respectively before applying any electric field. The molecules can switch between two domains when opposite electric fields are applied. We can see bright and dark states which are switchable alternately by using cross nicol polarizes.

3.2. Technical Merits

The principal advantages of SSFLCs from the practical point of view are fast electro optic response, the memory effect and the wide viewing angle.

(a) Fast Electro Optic Response

SSFLCs show very short switching time of μsec order because of the direct response of the spontaneous polarization for an electric field. This is about thousand times fast in comparison with the conventional nematic devices which utilize the dielectric anisotropy of molecule.

(b) Memory Effect

Both dark and bright states of SSFLCs shown in Figure 4 are stable respectively after when an electric field is removed. This memory effect is because of the surface anchoring effect and the fact that the both states are elastically equivalent. The memory effect is very important

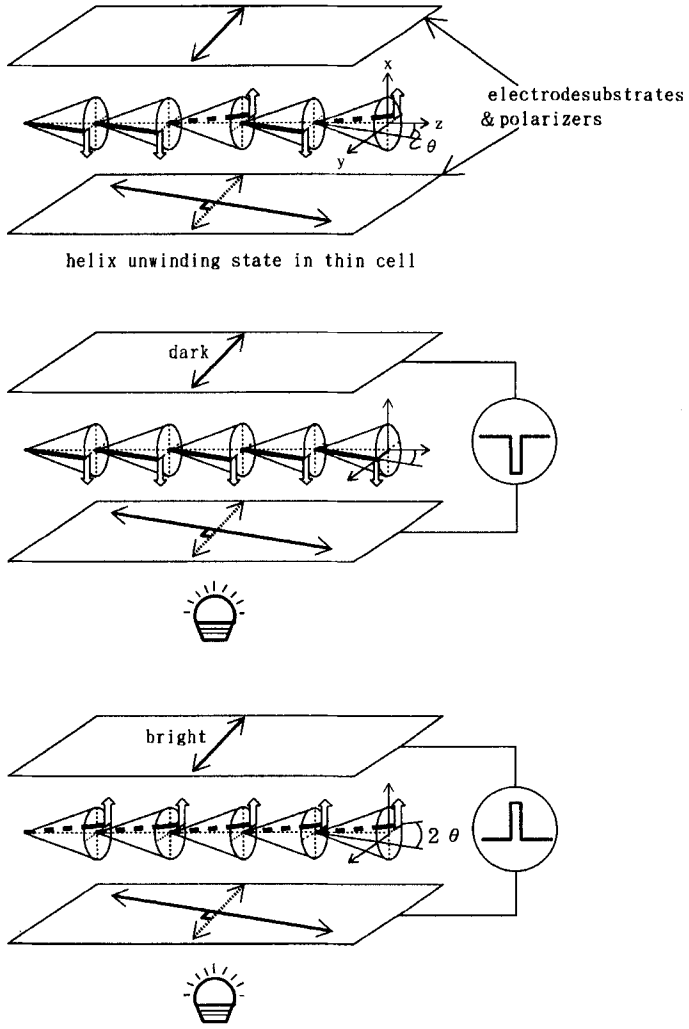

FIGURE 4 The principle device structure of SSFLC.

characteristic for a highly multiplexing display and an optical storage device.

(c) Wide Viewing Angle

The wide viewing angle is also a technical merit of SSFLCs. This is derived from the inplane molecular motions shown in Figure 4. The

viewing angular dependence of the effective birefringence is very slight under the inplane molecular motion. The wide viewing angle is important characteristic for the application like a large area display system watched from multi directions by a number of persons.

4. SMECTIC LAYER STRUCTURE STUDY

The discussion of the smectic layer structure is necessary before the molecular orientational study.

4.1. Smectic Layer Structures in Various Types of Alignment

The smectic layer structure strongly depends on the alignment. The smectic layer is formed to be parallel to the substrates in the homeotropic cell as shown in Figure 5, and the Schileren texture is observed under a polarizing microscope [3]. The oblique layer structure is formed in the planar homogeneous cell with the antiparallel alignment as shown in Figure 6 [4]. As shown in Figure 7, Rieker *et al.*, found the fact that the smectic layer structure in SSFLCs with the parallel alignment was the "Chevron" which bend like ≪, not the simple bookshelf structure by their X-ray study [5]. The smectic layer structure of SSFLCs with the parallel alignment except for a few unique FLC materials [6, 7] is characterized by the chevron structure [5, 8].

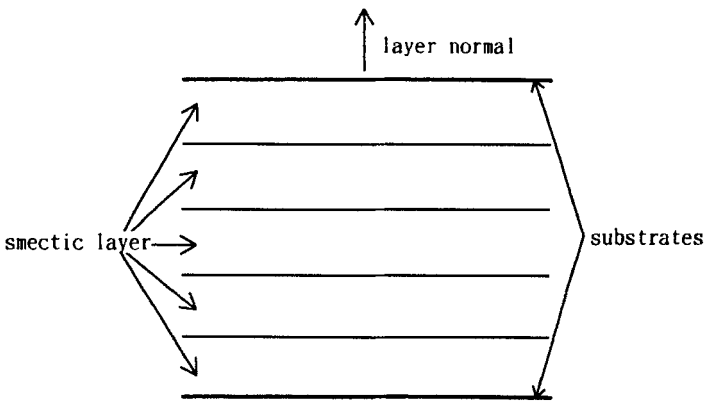

FIGURE 5 The smectic layer structure in the homeotropic cell.

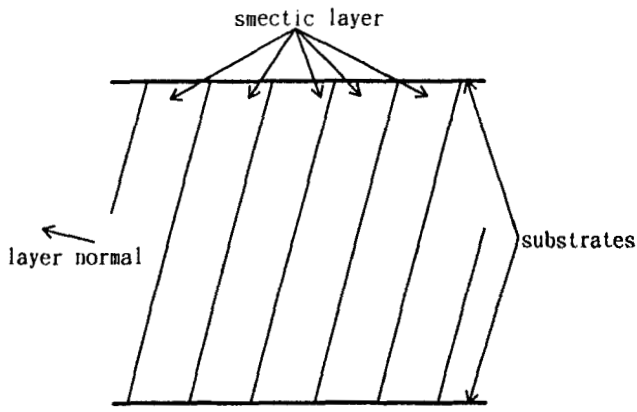

FIGURE 6 The smectic layer structure in the planar homogeneous cell with the antiparallel alignment. The oblique layer structure.

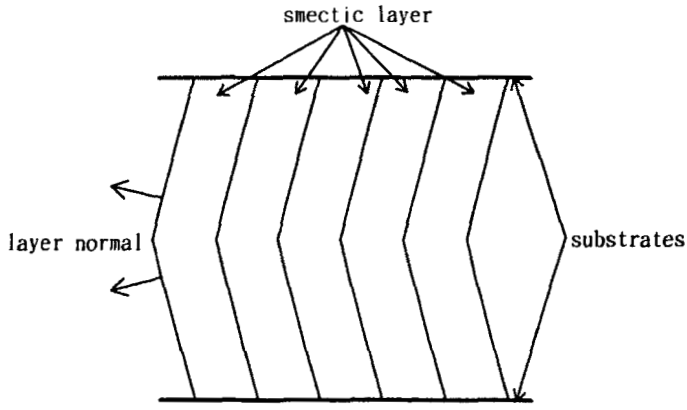

FIGURE 7 The smectic layer structure in the planar homogeneous cell with the parallel alignment. The chevron layer structure.

4.2. Relationship Between Molecular Tilt Angle and Chevron Layer Tilt Angle

The origin of the chevron layer structure is explained by discrepancy of the layer spacings between SmC* phase and it in high temperature phase which is usually SmA phase. The layer spacing in SmA phase, $d_{\wedge}$ is memorized at the surfaces, and it decreases to d_c in SmC* phase

because the molecules decline at the tilt angle θ from the smectic layer normal as shown in Figure 8. Figure 8 gives us a simple relation,

$$d_c = d_\Lambda \cos \delta_c, \tag{1}$$

where δ_c is the layer tilt angle in SmC* phase.

Figure 8 and Eq. (1) indicate that the layer tilt angle is equal to the molecular tilt angle. However some results that, for a few materials, the layer tilt angle is slightly smaller than the optically measured molecular tilt angle are reported [5, 7]. This discrepancy can be explained by recognizing the difference between the optical molecular tilt angle θ_{OPT}, resulting from the rigid central core, and the structural molecular tilt angle $\theta_{X\text{-}RAY}$, overall the zigzag molecular structure [9, 10] which includes the flexible alkyl chains. This is shown in Figure 9. The liquid crystal molecule is supposed to be a rod like structure as the first approximation. However in SmC* phase, the free rotation around the long molecular axis is hindered and the molecular structure is expressed by the zigzag model. It is possible to consider two types of zigzag model, $\theta_{OPT} > \theta_{X\text{-}RAY}$ and $\theta_{OPT} < \theta_{X\text{-}RAY}$.

The chevron layer structure of several SSFLCs were precisely investigated with various FLC materials exhibiting different optical

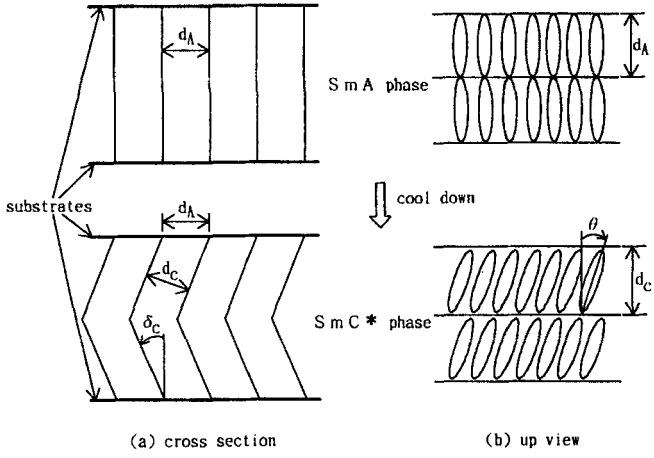

FIGURE 8 The explanation of origin of the chevron layer structure.

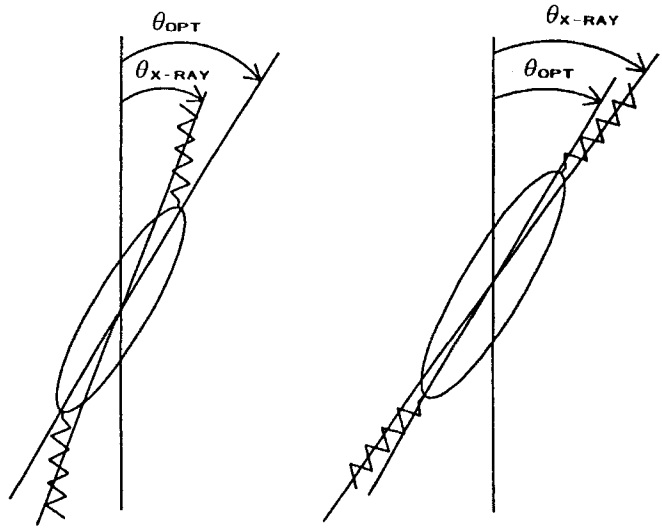

FIGURE 9 The zigzag molecular structure of SmC*.

molecular tilt angles, and a correlation between the layer tilt angle of the chevron structure and the optical molecular tilt angle were confirmed.

All measurements were performed at 25°C. The layer structure was measured by using X-ray scattering system Rigaku RU-200B (50 kV, 200 mA) having a Goniometer. The measurement geometry is shown in Figure 10. The Bragg diffraction angle is 2θ. The layer tilt angle is determined as the peak diffraction intensity position by β scanning. The micro cover glass plates about 150 μm thick were used in order to avoid X-ray absorption. The molecular tilt angles were measured observing the half of the two extinction positions of normal SSFLC cells having usual glasses with an ITO electrode when a square wave voltage ($\pm$ 10 V/μm, 1 Hz) was applied under cross nicol position of a polarizing microscope. This is the conventional method to measure the molecular tilt angle. It should be noted that the measured molecular tilt angle is the apparent tilt angle $\theta_{app.}$, differing from the real molecular tilt angle θ, half of the cone angle. The Cartesian coordinate system of the tilted layer structure is shown in Figure 11.

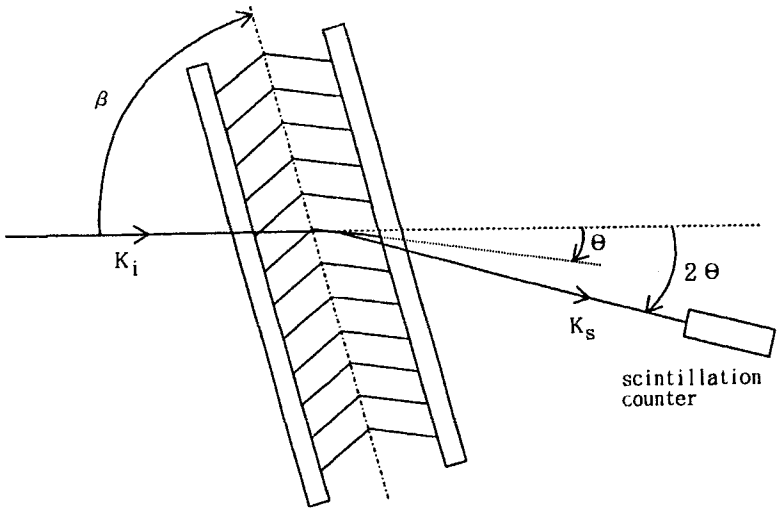

FIGURE 10 The scattering geometry of X-ray measurement.

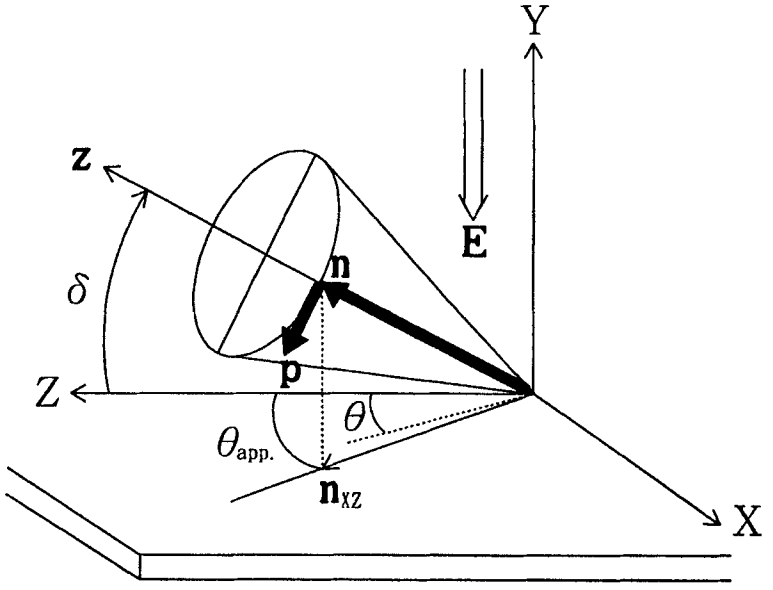

FIGURE 11 The coordinate system of the tilted layer structure. Here $\theta_{app.}$ is the apparent molecular tilt angle.

The layer is assumed to tilt in the YZ plane, where the vector $\mathbf{z}$ represents the perpendicular line of the cone. The FLC molecule is stabilized as the spontaneous polarization vector $\mathbf{p}$ becomes parallel to the YZ plane when an electric field $\mathbf{E}$ is applied along the Y axis. The apparent tilt angle $\theta_{\text{app.}}$ is the angle between the layer normal Z and the projection of the director $\mathbf{n}$ on the boundary XZ plane, $\mathbf{n}_{XZ}$, and is expressed as

$$\theta_{\text{app.}} = \tan^1(\tan\theta \cdot \sec\delta). \tag{2}$$

The optical molecular tilt angle was determined by Eq. (2).

FLC materials are shown in Table I with the transition temperature and the apparent tilt angle. Rieker *et al.* [5] and Ouchi *et al.* [8] reported that the layer tilt angle did not depend on the surface. A high pretilt polyimide PSI-A-2001 supplied by Chisso Co. Ltd., and a low pretilt PVA were used in order to reconfirm it. The rubbing direction was parallel and the cell thickness was nominally 2 μm. The pretilt angles θ_p were measured by capacitance-magnetic field (C-H) curves [11] using the antiparallel nominally 50 μm cells for nematic liquid crystal E. Merck E-8. The pretile angle of PSI-A-2001 was 15° and that of PVA was 0.5°.

The typical X-ray diffraction profiles are shown in Figure 12. Figure 12(a) shows the profile of mixture A with PSI-A-2001 and Figure 12(b)

TABLE I Physical properties of FLC materials used for X-ray study

FLC material	*Transition temperature/°C*				*Apparent tilt angle/°*
	$Cr \cdot S_C^*$	$\cdot S_\wedge$	$\cdot N$	$\cdot I$	(25°C)
Mixture A [a]	· < RT·	55·	82·	93	17
CS-1014 [b]	· < RT·	54·	69·	81	21
CS-1022 [c]	· < RT·	60·	73·	85	25
ZLI-3654 [d]	· < RT·	62·	76·	86	25
ZLI-3489 [e]	· < RT·	65·	71·	87	29
FELIX-002 [f]	· < RT·	70·	77·	87	33

[a] Blended by SHARP Co.
[b,c] Supplied by Chisso. Co. Ltd.
[d,e] Supplied by Chisso. Co. Ltd.
[f] Supplied by E. Merck.

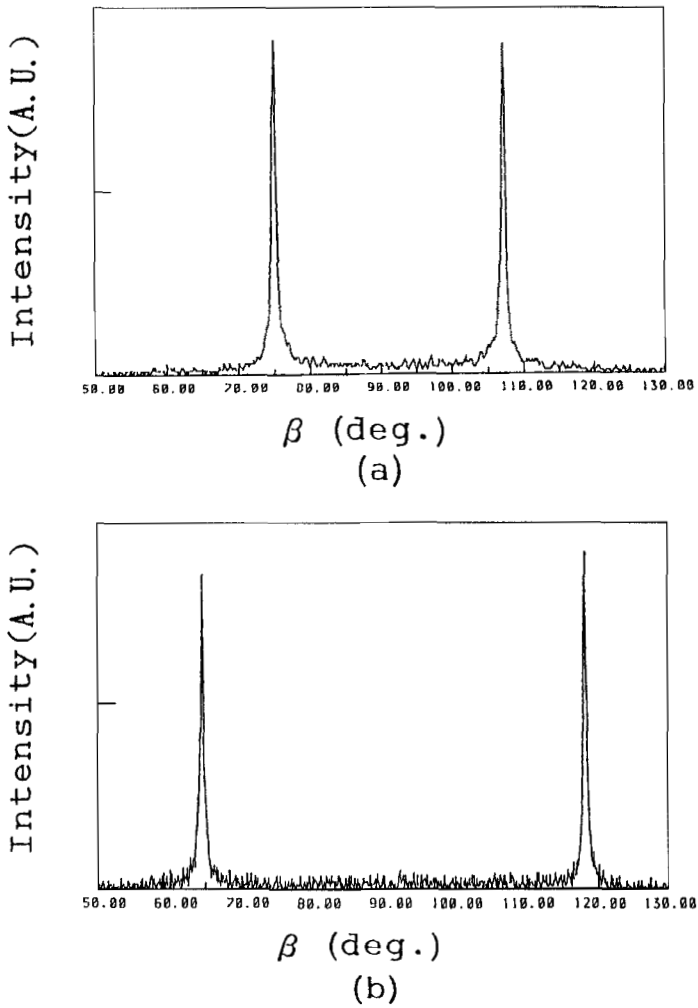

FIGURE 12 X-ray scattering profiles; (a) Mixture A with PSI-A-2001 and (b) FELIX-002 with PVA.

shows that of FELIX-002 with PVA. The peaks of all samples were sharp, and their positions and intensity were symmetric around the surface normal where β is 90°. The typical chevron layer structure was

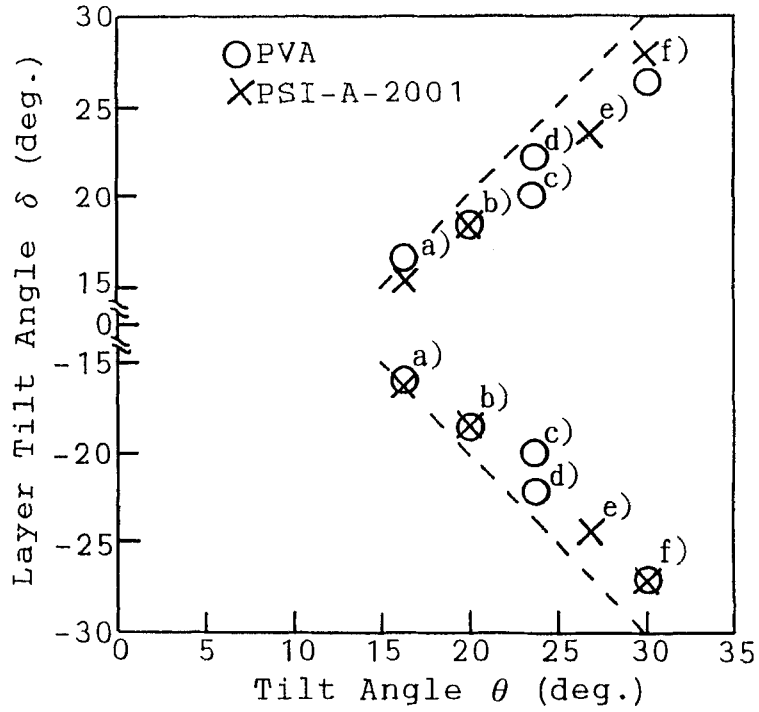

FIGURE 13 Relationship between the layer tilt angle and the molecular tilt angle. See text for explanation of figures.

formed in all SSFLC samples. Figure 13 shows the relationship between the tilt angle θ and the layer tilt angle δ. The circles and crosses with the letters (a)$\sim$(f) in Figures 13 and 14, represent the data of FLCs shown in Table I by identical letters. The dashed lines indicate the approximation that the layer tilt angle is equal to the tilt angle. It is found that the layer tilt angle is slightly smaller than the optical molecular tilt angle. Figure 14 shows the graph of the ratio κ ($= \delta/\theta$) *versus* θ. The variable $|\kappa|$ is around 0.9 and exhibits the tendency to gradually decrease as θ increases. A simple hypothesis can be considered that the zigzag molecular structure of FLCs showing a large molecular tilt angle is more marked than that of FLCs showing a small tilt angle, as shown in Figure 15. The difference between the aligning films were not recognized.

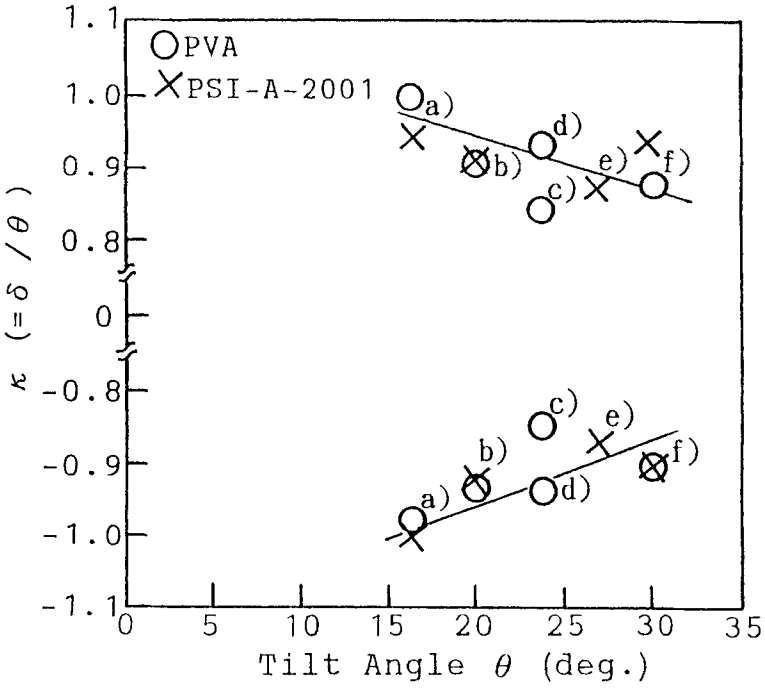

FIGURE 14 Correlation between the ratio of the layer tilt angle to the molecular tilt angle, κ and the molecular tilt angle. See text for explanation of figures.

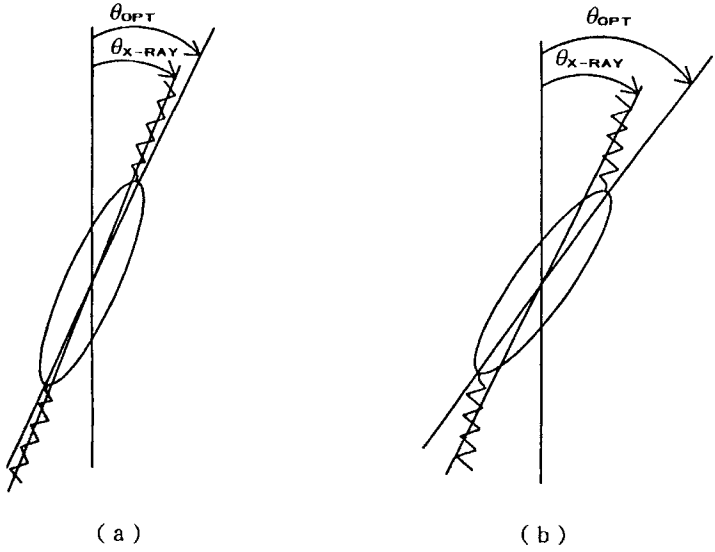

FIGURE 15 The zigzag molecular structure; (a) The material showing small molecular tilt angle. (b) The material showing large molecular tilt angle.

5. MOLECULAR ORIENTATIONAL STATES AND OPTICAL PROPERTIES

The molecular orientational states of SSFLCs were analyzed by using a polarizing microspectroscope and optical calculations. And the models of molecular orientation were presented, summarizing the orientational states of SSFLCs with the parallel rubbing. The X-ray study indicated that the chevron layer structure was determined by bulk properties of FLC, however, the molecular orientation in the smectic layer must be strongly influenced by the surface properties. The effect of the surface pretilt angle on the molecular orientation and optical properties of SSFLCs is discussed with regard to the simulation based on the molecular orientational models.

5.1. Classifications of the Molecular Orientational States

Two basic classifications of the molecular orientational states of SSFLCs were reported. One classification is based on the optical viewing behavior when SSFLCs are placed between cross nicol polarizers. The uniform (U) and twisted (T) states are defined by this classification [12, 13]. The uniform state shows extinction positions, but the twisted state shows only coloration positions without any extinction. Other classification is based on the relationship between the tilting direction of the chevron layer structure and the direction of the surface pretilt. The C1 and C2 states are defined by this classification [14]. The C1 and C2 states are easily distinguished because the tilting direction of the chevron layer structure is confirmed by the direction of the zigzag defects [15, 16], and the direction of the surface pretilt is consistent with the rubbing direction [17]. The zigzag defect is caused by discontinuity of the chevron layer structure. Figures 16(a) and 16(b) show the C1 and C2 states related with the zigzag defect. Figure 16(c) shows the smectic layer models of the C1 and C2 states.

The four states, C1U (C1-uniform), C1T (C1-twisted), C2U (C2-uniform) and C2T (C2-twisted) were found in SSFLC cells by investigating a lot of samples aligned by various aligning films with the parallel rubbing [18]. These four states are expressed by the combination of above two classifications.

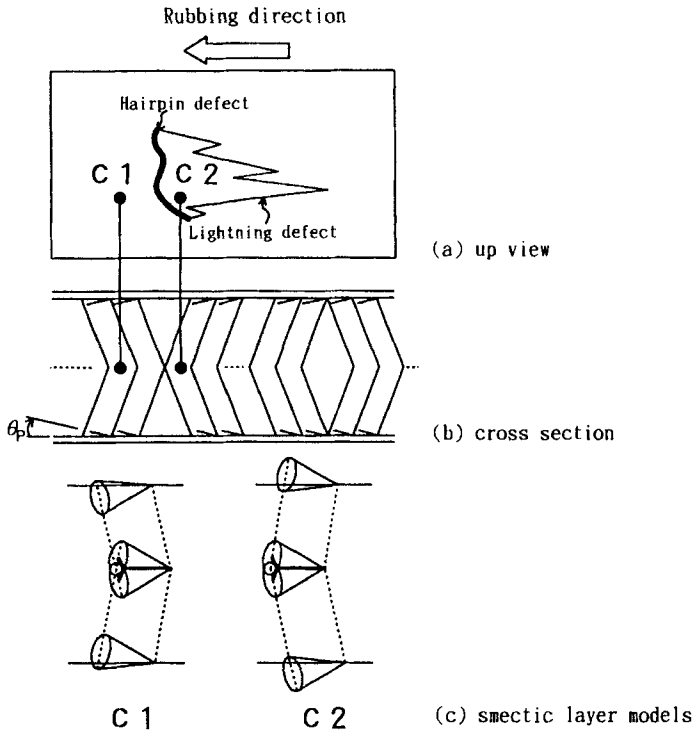

FIGURE 16 The C1 and C2 states, distinguished by the relationship between the direction of the chevron layer structure and the direction of the surface pretilt, as shown in (a) and (b). The tilting direction of the chevron layer structure is confirmed by the direction of the zigzag defects, as shown in (b). (c) The smectic layer models of the C1 and C2 states.

5.2. Experimental and Results

FLC materials are shown in Table II with the apparent tilt angle, the layer tilt angle and the tilt angle. Aligning films are shown in Table III with the baking temperature and the surface pretilt angle. The aligning films are all polyimide. As it is known that the baking temperature of polyimide affects the pretilt angle [19], the baking temperatures are shown in Table III. SSFLC cells were mounted in a hot stage and positioned between cross nicol polarizing microscope. The memory angle θ_m was defined as the half angle between two extinction positions when no field was applied. A spectroscope is attached to a polarizing

TABLE II Tilt angles and layer tilt angles of FLC materials used for molecular orientational study at 25°C

FLC material	*Apparent tilt angle/°*	*Layer tilt angle/°*	*Tilt angle/°*
CS-1014 [a]	21.0	18.0	20.0
SF-1212 [b]	9.5	9.0	9.4
SCE-8 [c]	22.0	19.5	21.0

[a] Supplied by Chisso Co. Ltd.
[b] SHARP's blending mixture.
[c] Supplied by E. Merck.

TABLE III Baking temperatures and pretilt angles of aligning films used for molecular orientation study

Aligning film [a]	*Baking temperature/°C*	*Pretilt angle/°*
PI-X	200	3
PSI-A-2101	200	6
PSI-A-X018	250	10
PI-Z	250	10
PSI-A-2001	200	15
PSI-A-X021	250	20

[a] All aligning films were supplied by Chisso Co. Ltd.

microscope in order to measure the transmitted light of small areas, such as the inside of the zigzag defect.

The different orientational states of SSFLCs with the different aligning films for the same FLC are shown. Figure 17 shows the polarized optical micrographs of the cell used with FLC CS-1014 and the high pretilt aligning film PSI-A-2001 ($\theta_p = 15°$). Figure 18 shows the micrographs of the cell used with CS-1014 and the low pretilt aligning film PI-X ($\theta_p = 3°$). Both micrographs were taken in the crossed nicol position at 25°C. The C1 and C2 states are identified on each side of the zigzag defects. The layer normal is parallel to the polarizer in Figures 17(a) and 18(a). Figures 17(b) and 18(b) show the viewing states when the cells are rotated from the positions of Figures 17(a) and 18(a), respectively. Only the C2 state shows the extinction position (C2U) in Figure 17(b), and the C2 state showed only the C2U state everywhere in this PSI-A-2001's cell. Both the C1 and C2 states show the extinction position (C1U and C2U) in Figure 18(b). Figure 17(c) shows the viewing state when the cell is rotated further from the position of Figure 17(b). Only the C1 state showed the extinction position

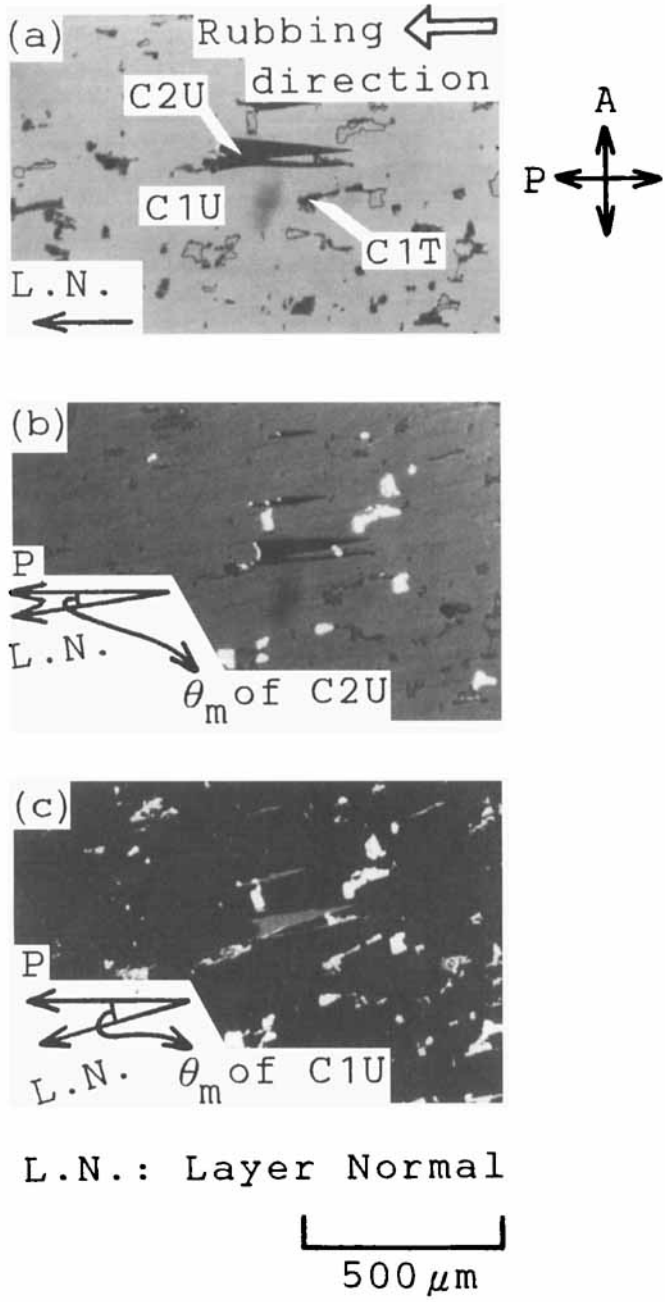

FIGURE 17 The polarized optical micrographs of the sample used with CS-1014 and high pretilt aligning film PSI-A-2001. See text for explanation. L.N. denotes the layer normal.

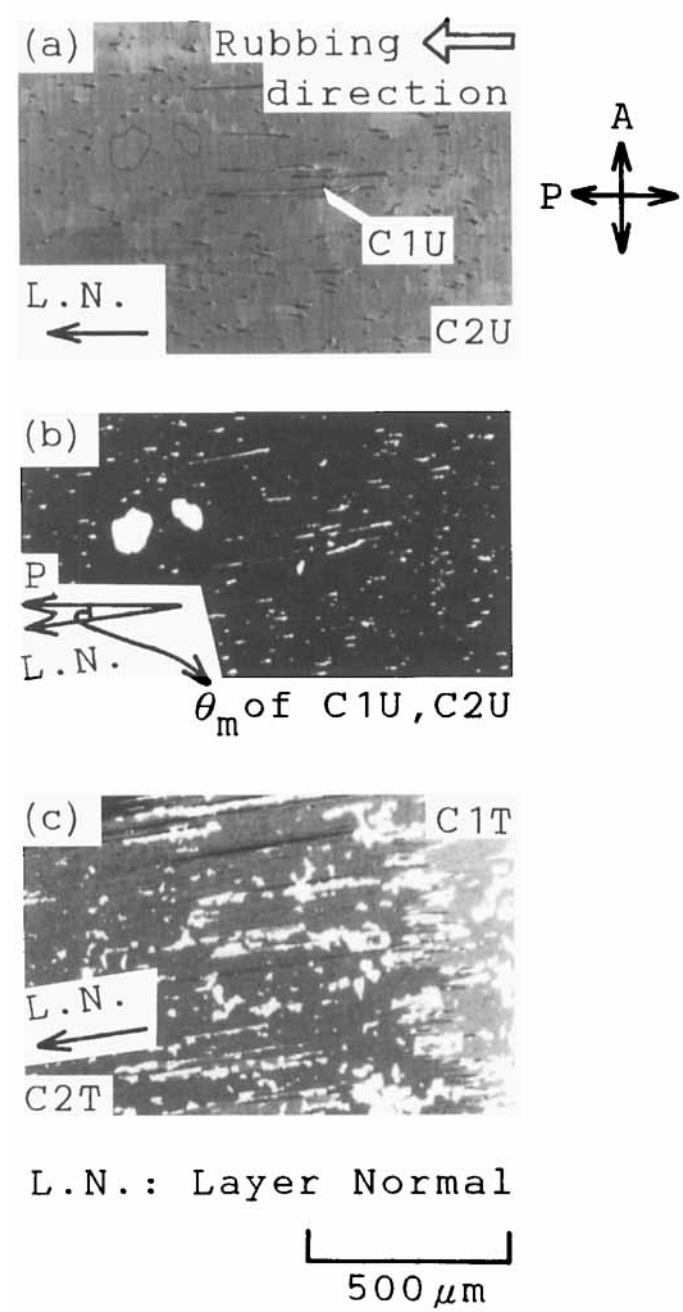

FIGURE 18 The polarized optical micrographs of the sample used with CS-1014 and low pretilt aligning film PI-X. See text for explanation. L.N. denotes the layer normal.

(C1U) at this position, and the small C1 state without any extinction position (C1T) were seen. Figure 18(c) shows another area of the cell. Both the C1 and C2 states showed only coloration positions without any extinction positions (C1T and C2T) in this area. From Figures 17 and 18, it is found that the four states, C1U, C1T, C2U and C2T can appear in SSFLCs with the parallel rubbing, and that SSFLCs with high pretilt aligning films show only one state with extinction positions in the C2 state. This type of the C2 state is defined as a special case of the C2U state, called the high pretilt C2U state. On the other hand, both the C1U and C1T states can appear regardless of the pretilt angle. The C1U and C2U states are interesting from the practical point of view because they have possibility to achieve a high contrast.

The memory angles of the C1U and C2U states are shown schematically in Figures 17 and 18. The memory of the C1U state is greater than that of the C2U state in the high pretilt cell (Figs. 17(b) and 17(c)). However, the difference between the memory angles of the C1U and C2U states is very small in the low pretilt cell (Fig. 18(b)). It is expected that the memory angle depends on the surface pretilt angle. The temperature dependences of the memory angles of the C1U and C2U states were measured for all cells, and are shown in Figure 19. The solid lines represent the apparent tilt angle behavior. There is little difference in the apparent tilt angles among the cells, indicating the reliability of the cells. Some cells used with FLC SF-1212, and aligning films except for PI-X and PSI-A-2101, showed only the C1 state with slight zigzag defects. According to Kanbe *et al.* [14], it is difficult for the C2 state to appear if the titt angle is small or the surface pretilt angle is high. The memory angle of the C2U state was almost independent of the aligning films. The memory angle of the C1U state strongly depended on the aligning films.

The optical properties of SSFLC cell used with CS-1014 and PSI-A-2001, were measured in order to analyze the molecular orientations. The wavelength dependences of the memory angles of the C1U and C2U states are shown in Figure 20. The C1U and C2U states exhibit the opposite wavelength dispersion with respect to each other. The transmission spectra of both memory states, the bright and dark states, prepared by applying a pulsed electric field, are shown in Figure 21. The transmission spectra indicate that a high contrast ratio is obtained not by the C2U state, but by the C1U state. The large memory angle

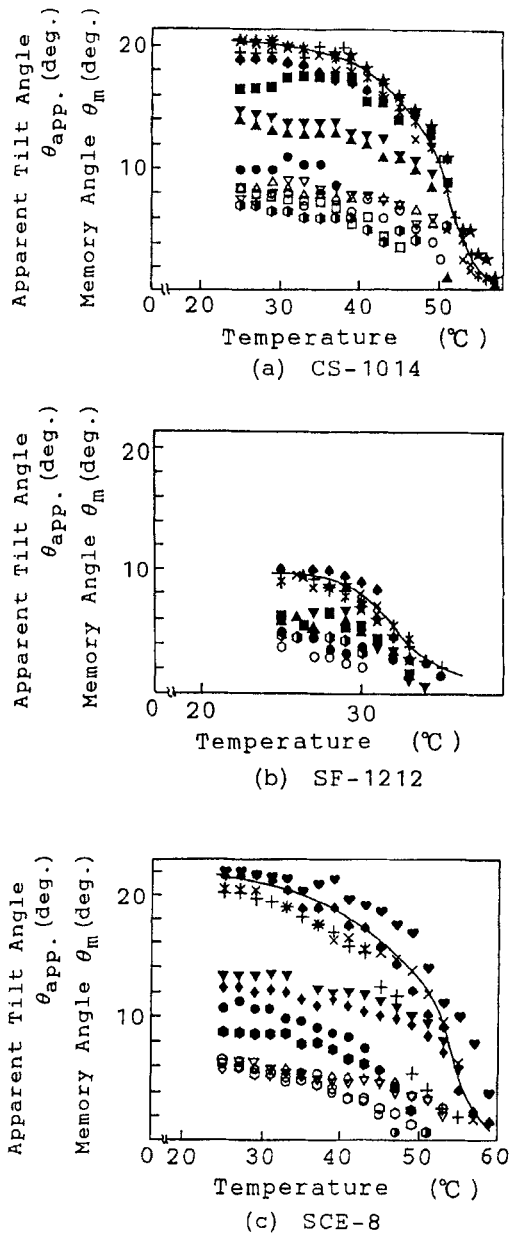

FIGURE 19 The temperature dependence of the apparent tilt angle (♠, +, ×, ♥, *, ★,), the memory angle of the C1U state (⬟, ●, ▲, ◆, ▼, ■) and the memory angle of the C2U state (○, ○, △, ◇, ▽, □) with various aligning films PI-X (♠, ⬟, ○), PSI-A-2101 (+, ●, ○), PSI-A-X018 (×, ▲, △), PI-Z (♥, ◆, ◇), PSI-A-2001 (*, ▼, ▽) and PSI-A-X021 (★, ■, □) for (a) CS-1014, (b) SF-1212 and (c) SCE-8. The lines are the apparent tilt angle behavior.

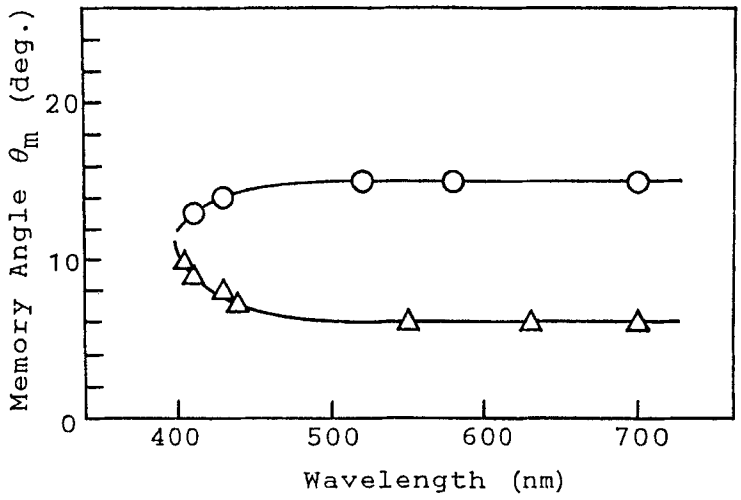

FIGURE 20 The wavelength dependences of the memory angle of the C1U state (○) and the C2U state (△).

contributed to a high contrast ratio. The transmitted light was calculated theoretically in order to discuss these optical properties.

The molecular orientational models of the C1U, C1T, C2U, C2T and the high pretilt C2U states are shown in Figure 22. The molecules are almost uniformly tilted at one side from the layer normal in the C1U and C2U models. The C1T and C2T models are the half splayed states [20, 21]. The boundary surfaces in the C2 state do not have wide regions wherein the molecules can exist stably, as shown in Figure 16. The *c*-directors at the surfaces are almost perpendicular to the substrate in the high pretilt C2U model. The molecules at surfaces can move easily even in the C2 state if the pretilt is low. These states are assumed to switch between two elastically equivalent states for the stable memory effect.

Figure 23 shows the coordinate systems. In Figure 23, **n** is the director, **c** is the c-director and **p** is the spontaneous polarization vector. It is assumed that the tilt angle θ and the layer tilt angle δ are constant, and the azimuthal angle Φ depends only on the cell thickness direction Y. The director is expressed as follows:

$$\mathbf{n}(x, y, z) = (\sin\theta\cos\Phi, \sin\theta\sin\Phi, \cos\theta), \tag{3}$$

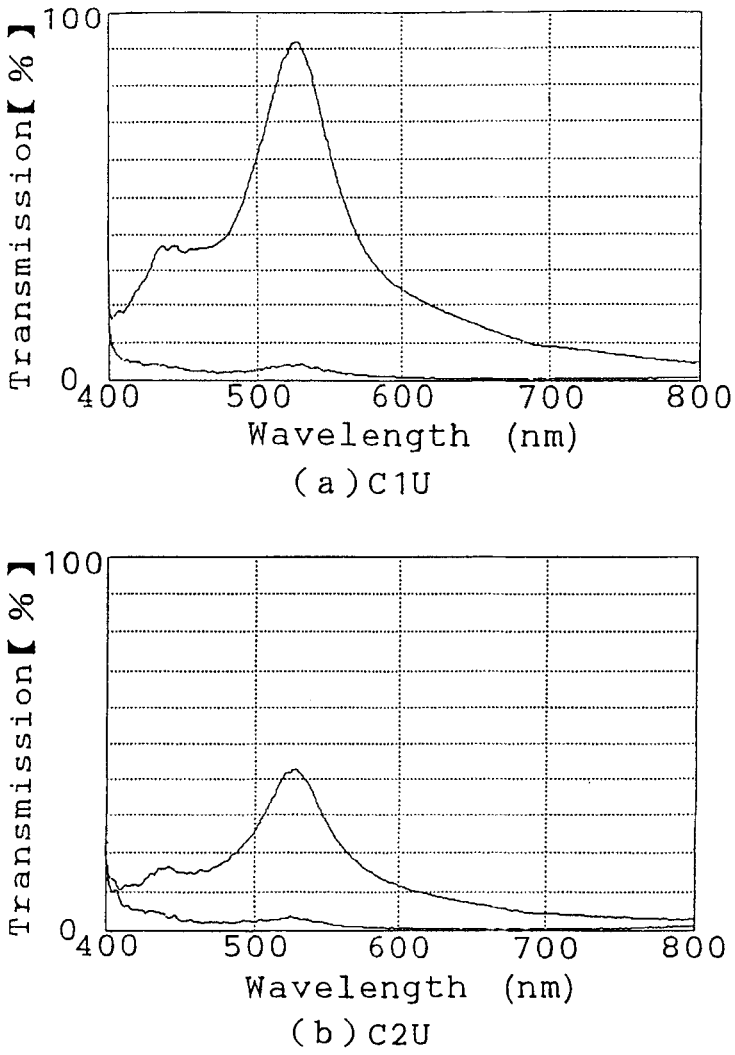

FIGURE 21 The transmission spectra of the (a) C1U and (b) C2U memory states. The upper curves represent the bright spectra and the bottom curves represent the dark spectra.

and

$$\mathbf{n}(X,Y,Z) = \begin{pmatrix} \sin\theta & \cos\Phi & & \\ \sin\theta & \sin\Phi & \cos\delta - \cos\theta & \sin\delta \\ \sin\theta & \sin\Phi & \sin\delta + \cos\theta & \cos\delta \end{pmatrix}. \qquad (4)$$

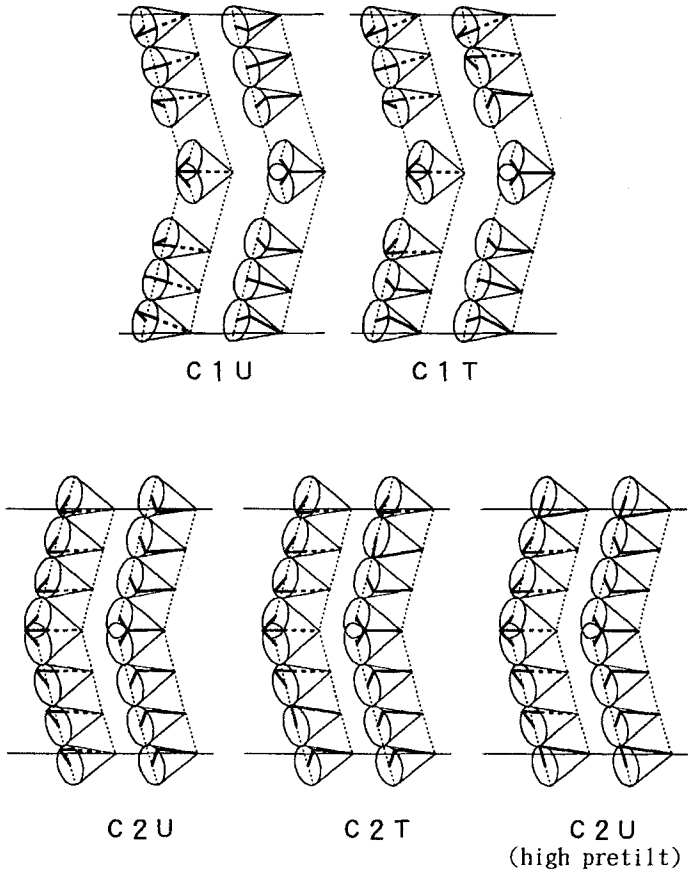

FIGURE 22 The molecular orientational models of SSFLCs, possessing a chevron layer structure.

The transmitted light was calculated by the Berreman 4×4 matrix method [22]. The dielectric tensor is determined by the director tilt angle γ and the director twist angle ϕ which are expressed as

$$\gamma = \sin^{-1}(\sin\theta \sin\Phi \cos\delta - \cos\theta \sin\delta), \tag{5}$$

$$\phi = \tan^{-1}\left(\frac{\sin\theta \cos\Phi}{\sin\theta \sin\Phi \sin\delta + \cos\theta \cos\delta}\right). \tag{6}$$

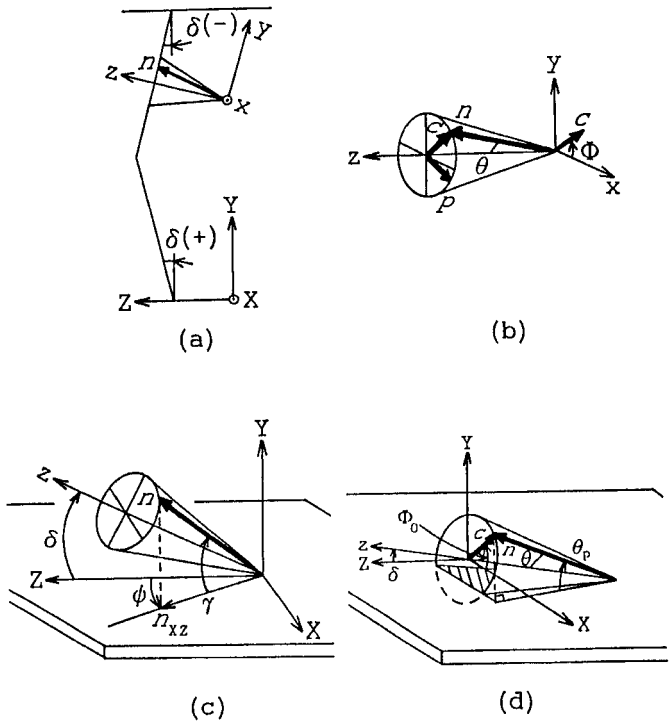

FIGURE 23 The coordinate systems used for calculations. Y and Z represent the cell thickness direction and the smectic layer normal, respectively, and z is the perpendicular line of cone. (a) The chevron layer system. (b) The cone system. (c) The director tilt angle γ and the director twist angle ϕ. (d) The scheme of the director at the surface.

The pretilt angle θ_p is simply defined as Figure 23(d). The c-director pretilt Φ_0 is expressed by Eq. (7)

$$\Phi_0 = \sin^{-1}\left(\frac{\tan\delta}{\tan\theta} + \frac{\sin\theta_p}{\sin\theta\cos\delta}\right). \tag{7}$$

It is assumed that Φ_0 at the bottom surface is $\pi/2$ and Φ_0 at the top surface is $-\pi/2$ for the high pretilt C2U. The azimuthal angle at the chevron interface Φ_{1N} is expressed as

$$\Phi_{1N} = \sin^{-1}(\tan\delta/\tan\theta). \tag{8}$$

For simplicity, it is assumed that Φ changes with Y at a constant rate, ignoring the effect of the polarization electric field on the elastic

deformation [23]. After Kawaida *et al.* [24], the wavelength dispersion of the refractive indices was taken into account. The wavelength dependences of the memory angles and the transmission spectra were calculated for CS-1014 ($\theta = 20.0°, \delta = 18.0°$) and PSI-A-2001 ($\theta_p = 15°$).

The calculated wavelength dependences of the memory angles are shown in Figure 24. Both the C1U and C2U models exhibit the same dispersion as the experimental results. Figure 25 shows the calculated transmission spectra. Both the C1U and C2U models show slight transmission in short wavelength regions of the dark states, and show a peak transmission around 500 nm of the bright states. The calculated results were almost consistent with the experimental results, indicating the approximate validity of the orientational models. The dependences of the memory angles on the surface pretilt angle were simulated using the models, and are shown in Figure 26 with the experimental results of Figure 19 at 25°C. In every case, the calculated memory angle is the value of wide visible wavelengths. For every material, good agreement between the simulated and the experimental results was confirmed.

The director profiles were calculated in order to discuss above results. All calculations were performed for CS-1014. In Figure 27, the

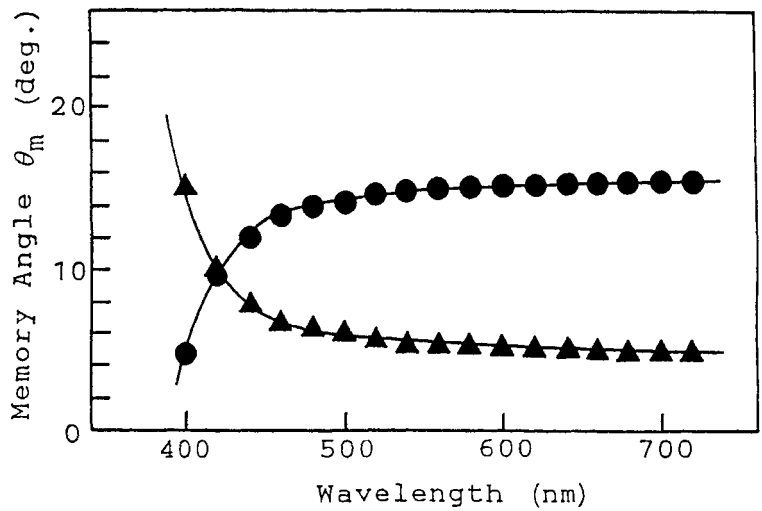

FIGURE 24 The calculated wavelength dependences of the memory angle of the C1U state (●) and the C2U state (▲).

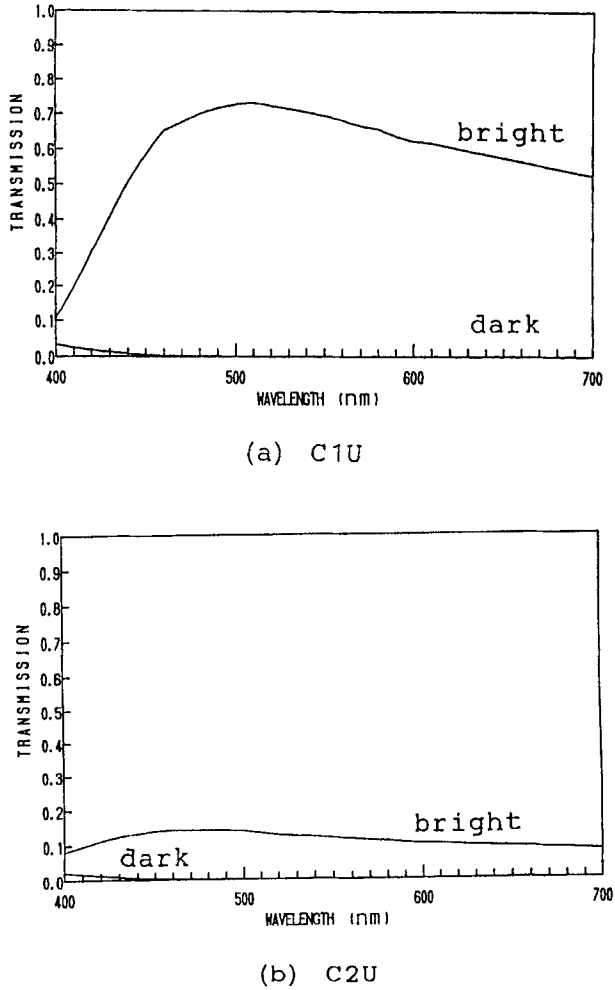

FIGURE 25 The calculated transmission spectra of the (a) C1U and (b) C2U state.

director twist angle ϕ is shown as a function of the cell thickness direction Y for various surface pretilt angles, where ϕ_{1N} represents the director twist angle at the chevron interface and is expressed as

$$\phi_{1N} = \cos^{-1}(\cos\theta/\cos\delta). \tag{9}$$

The memory angles of each case are indicated simultaneously in Figure 27. In Figure 28, the calculated transmission spectrum for each

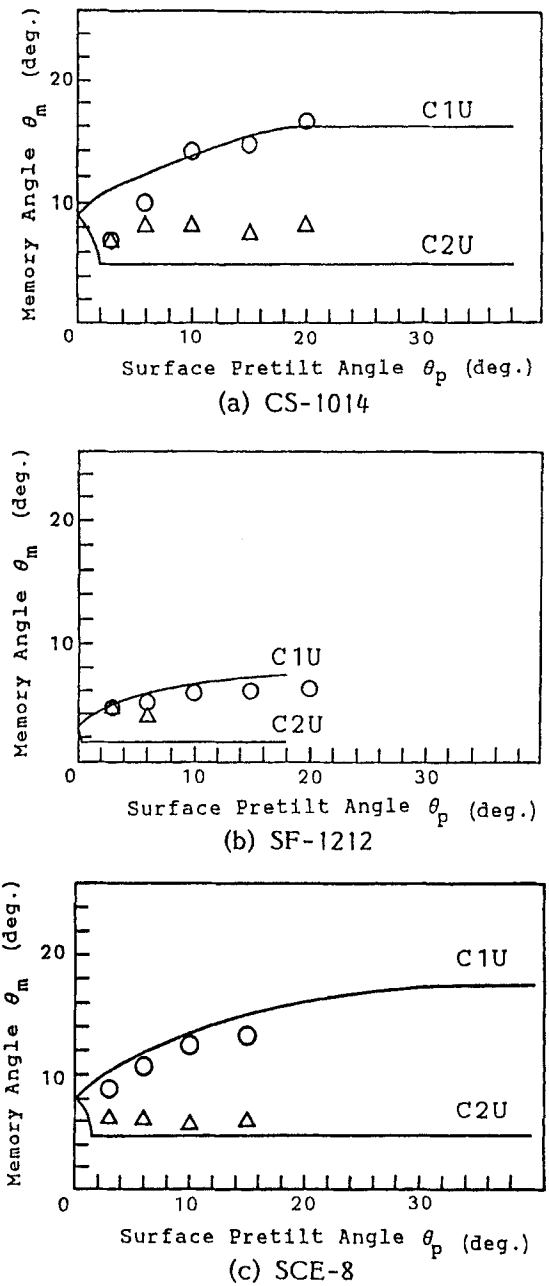

FIGURE 26 The relationships between the surface pretilt angle and the memory angle of the C1U state (○), and the C2U state (△) for (a) CS-1014, (b) SF-1212 and (c) SCE-8.

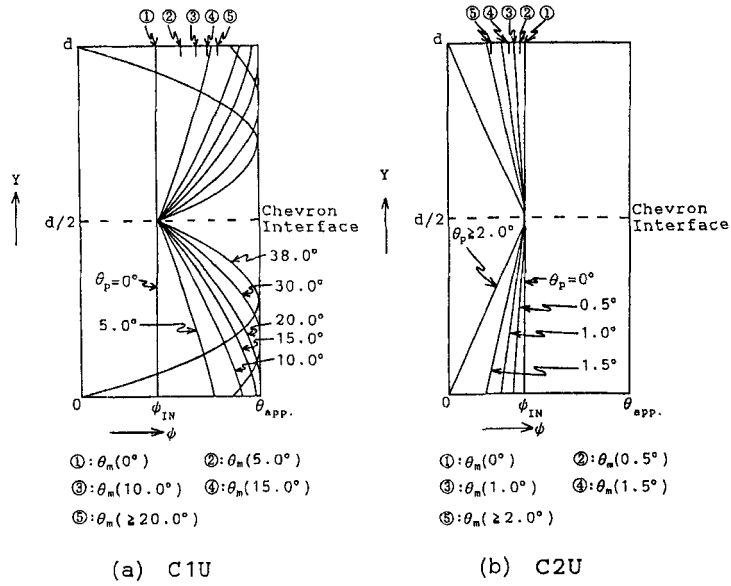

FIGURE 27 The calculated director profiles and the memory angles for various surface pretilt angles for the (a) C1U and (b) C2U states. The memory angles are denoted by encircled numerals; In (a), 1 : $\theta_m(\theta_p = 0°)$, 2 : $\theta_m(\theta_p = 5.0°)$, 3 : $\theta_m(\theta_p = 10.0°)$, 4 : $\theta_m(\theta_p = 15.0°)$ and 5 : $\theta_m(\theta_p \geqq 20.0°)$; In (b), 1 : $\theta_m(\theta_p = 0°)$, 2 : $\theta_m(\theta_p = 5.0°)$, 3 : $\theta_m(\theta_p = 1.0°)$, 4 : $\theta_m(\theta_p = 1.5°)$ and 5 : $\theta_m(\theta_p \geqq 2.0°)$.

case is shown. These figures indicate that the memory angle and the transmission of the bright state depend on the surface pretilt angle.

It is found that the memory angle θ_m is determined by the following equation,

$$\theta_m = (\phi_0 + \phi_{1N})/2, \tag{10}$$

where ϕ_0 is the director twist angle at the surface. The memory angle of the C1U state becomes large by increasing the surface pretilt angle and saturates at values of $\theta_{msat.}$ expressed as Eq. (11).

$$\theta_{msat.} = (\phi_{1N} + \theta_{app.})/2. \tag{11}$$

On the other hand, the memory angle of the C2U state becomes large by decreasing the surface pretilt angle. The results in Figure 26 are well explained by the orientational models. However, the memory angle of the C2U state seems to be virtually constant because its surface pretilt dependence is very slight.

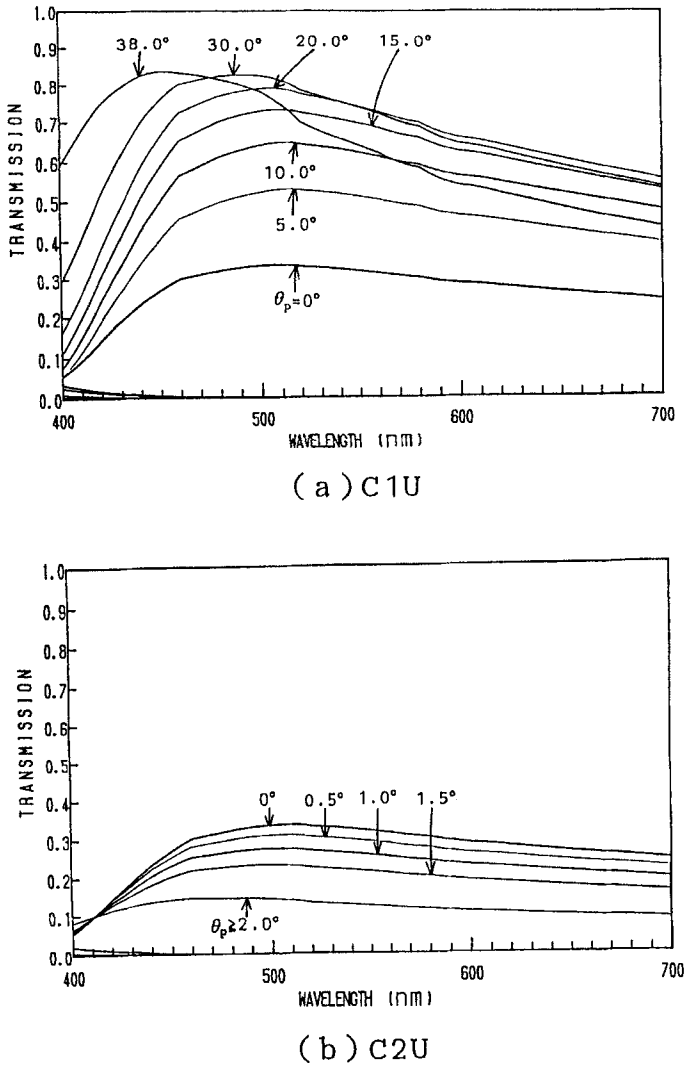

FIGURE 28 The calculated transmission spectra for various surface pretilt angles of the (a) C1U and (b) C2U states.

6. CONCLUSION

The orientational states which appear in SSFLC cells with the parallel rubbing are summarized in Figure 29, expressed by the c-director

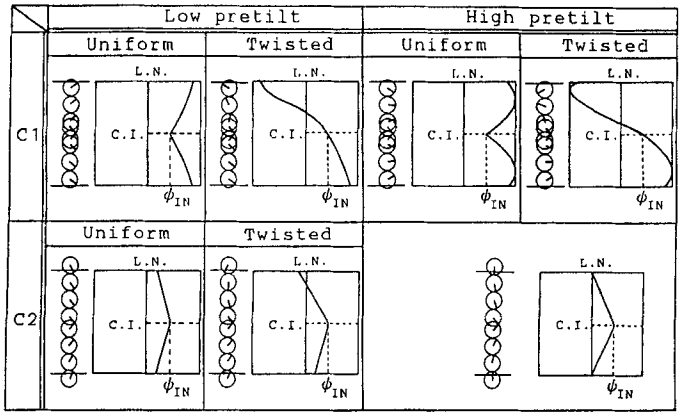

FIGURE 29 A summary of the orientational states in SSFLCs with the chevron layer structure.

orientations and director profiles. The different optical properties are shown by these molecular orientational states even in a SSFLC cell with one FLC materal. An understanding of the molecular orientational states using by the molecular orientational models is very important not only for the practical applications but also to enable reliable experiments of SSFLC.

Finally, author will be happy if the concept and the procedure of this study is interesting and useful for the polymer liquid crystals research.

References

[1] Meyer, R. B., Liébert, L., Strzelecki, L. and Keller, P. (1975). *J. Phys.*, **36**, L69.
[2] Clark, N. A. and Lagerwall, S. T. (1980). *Appl. Phys. Lett.*, **36**, 899.
[3] Gray, G. W. and Goodby, J. W. (1984). *Smectic Liquid Crystals* (Leonard Hill).
[4] Ouchi, Y., Lee, J., Takezoe, H., Fukuda, A., Kondo, K., Kitamura, T. and Mukoh, A. (1988). *Jpn. J. Appl. Phys.*, **27**, L1993.
[5] Rieker, T. P., Clark, N. A., Smith, G. S., Parmar, D. S., Sirota, E. B. and Safinya, C. R. (1987). *Phys. Rev. Lett.*, **59**, 2658.
[6] Mochizuki, A., Yoshihara, T., Iwasaki, M., Nakatsuka, M., Takanishi, Y., Ouchi, Y., Takezone, H. and Fukuda, A. (1990). *Proceedings of the SID*, **31**, 123.
[7] Takanishi, Y., Ouchi, Y., Takezoe, H., Fukuda, A., Mochizuki, A. and Nakatsuka, M. (1990). *Jpn. J. Appl. Phys.*, **29**, L984.
[8] Ouchi, Y., Lee, J., Takezoe, H., Fukuda, A., Kondo, K., Kitamura, T. and Mukoh, A. (1988). *Jpn. J. Appl. Phys.*, **27**, L725.
[9] Goodby, J. W. and Chin, E. (1986). *J. Am. Chem. Soc.*, **108**, 4736.
[10] Keller, E. N., Nachaliel, E. and Davidov, D. (1986). *Phys. Rev. A*, **34**, 4363.

[11] Suzuki, K., Toriyama, K. and Fukuhara, A. (1978). *Appl. Phys. Lett.*, **33**, 561.
[12] Handschy, M. A., Clark, N. A. and Lagerwall, S. T. (1983). *Phys. Rev. Lett.*, **51**, 471.
[13] Ouchi, Y., Takezoe, H. and Fukuda, A. (1987). *Jpn. J. Appl. Phys.*, **26**, 1.
[14] Kanbe, J., Inoue, H., Mizutome, A., Hanyuu, Y., Katagiri, K. and Yoshihara, S. (1991). *Ferroelectrics*, **114**, 3.
[15] Ouchi, Y., Takano, H., Takezoe, H. and Fukuda, A. (1988). *Jpn. J. Appl. Phys.*, **27**, 1.
[16] Clark, N. A. and Rieker, T. P. (1988). *Phys. Rev. A*, **37**, 1053.
[17] Okano, K. and Kobayashi, S. (1985). Ekisyo Oyohen (Application of Liquid Crystals) [in Japanese] (Baihukan Press).
[18] Koden, M., Katsuse, H., Tagawa, A., Tamai, K., Itoh, N., Miyoshi, S. and Wada, T. (1992). *Jpn. J. Appl. Phys.*, **31**, 3632.
[19] Tagawa, A., Katsuse, H., Tamai, K., Itoh, N., Koden, M., Miyoshi, S. and Wada, T. (1992). *Proc. of Japan Display 1992*, p. 519.
[20] Maclennan, J. E., Clark, N. A., Handschy, M. A. and Meadows, M. R. (1990). *Liquid Crystals*, **7**, 753.
[21] Elston, S. J. and Sambles, J. R. (1990). *Jpn. J. Appl. Phys.*, **29**, L641.
[22] Berreman, D. W. (1972). *J. Opt. Soc. Am.*, **62**, 502.
[23] Nakagawa, M. and Akahane, T. (1986). *J. Phys. Soc. Jpn.*, **55**, 1516.
[24] Kawaida, M., Yamaguchi, T. and Akahane, T. (1989). *Jpn. J. Appl. Phys.*, **28**, L1602.